
EEG EMOTION CLASSIFICATION USING AN ENHANCED TRANSFORMER-CNN-BILSTM ARCHITECTURE WITH DUAL ATTENTION MECHANISMS

S M Rakib UI Karim

Dept. of Electrical & Computer Engineering
University of Missouri
Columbia, Missouri, United States
skarim@missouri.edu

Wenyi Lu

Dept. of Computer Science
University of Missouri
Columbia, Missouri, United States
w1dh6@mail.missouri.edu

Diponkor Bala

Dept. of Computer Science & Engineering
City University
Savar, Bangladesh
diponkor.b@gmail.com

Rownak Ara Rasul

Dept. of Computer Science
University of Missouri
Columbia, Missouri, United States
rrasul@missouri.edu

Sean Goggins

Dept. of Electrical & Computer Engineering
University of Missouri
Columbia, Missouri, United States
goggins@missouri.edu

February 9, 2026

ABSTRACT

Electroencephalography (EEG)-based emotion recognition plays a critical role in affective computing and emerging decision-support systems, yet remains challenging due to high-dimensional, noisy, and subject-dependent signals. This study investigates whether hybrid deep learning architectures that integrate convolutional, recurrent, and attention-based components can improve emotion classification performance and robustness in EEG data. We propose an enhanced hybrid model that combines convolutional feature extraction, bidirectional temporal modeling, and self-attention mechanisms with regularization strategies to mitigate overfitting. Experiments conducted on a publicly available EEG dataset spanning three emotional states (neutral, positive, and negative) demonstrate that the proposed approach achieves state-of-the-art classification performance, significantly outperforming classical machine learning and neural baselines. Statistical tests confirm the robustness of these performance gains under cross-validation. Feature-level analyses further reveal that covariance-based EEG features contribute most strongly to emotion discrimination, highlighting the importance of inter-channel relationships in affective modeling. These findings suggest that carefully designed hybrid architectures can effectively balance predictive accuracy, robustness, and interpretability in EEG-based emotion recognition, with implications for applied affective computing and human-centered intelligent systems.

1 Introduction

Electroencephalography (EEG) enables non-invasive, high-temporal-resolution decoding of neural activity and is widely explored for emotion recognition in affective computing, mental health assessment, and adaptive human-computer

interfaces [1, 2]. Distinct oscillatory and connectivity patterns reflect emotional states such as neutral, positive, and negative [3, 4], offering opportunities for objective affect monitoring. However, practical deployment remains challenging due to high dimensionality, subject variability, and non-stationarity in EEG signals [5].

Early pipelines relied on handcrafted statistical, spectral, and connectivity features combined with classifiers such as SVMs and Random Forests [6, 3], achieving moderate performance while requiring extensive feature engineering and offering limited interpretability [7]. Deep learning has improved decoding by learning spatial and temporal representations directly from data: CNNs extract spatial structure [8], BiLSTMs capture temporal dependencies [9, 10], and transformer-based attention mechanisms model long-range dependencies [11, 12]. Although attention-based graph and spatial-temporal models have achieved strong benchmark performance [13, 14, 15], gaps remain in multi-stage attention design, bidirectional temporal modeling, systematic feature analysis, and statistical benchmarking against strong baselines. To address these gaps, we investigate the following research questions (RQs):

- **RQ1:** To what extent do hybrid deep learning architectures that integrate convolutional, recurrent, and attention-based components improve EEG-based emotion classification performance, robustness to overfitting, and interpretability compared to classical and deep learning baselines?
- **RQ2:** Which categories of EEG features (statistical, frequency-domain, covariance, and eigenvalue-based) contribute most strongly to emotion discrimination?

We propose an Enhanced Transformer-CNN-BiLSTM hybrid architecture featuring residual 1D CNN blocks, dual BiLSTMs, and dual multi-head self-attention modules (16+8 heads) with advanced regularization (dropout, layer normalization, label smoothing, weight decay) to improve generalization and interpretability. On a 2,529-sample EEG dataset with 988 features across three emotion classes, the model achieves 99.19% validation accuracy with only a 0.56% train-validation gap, substantially outperforming classical models and a standard hybrid Transformer-CNN-BiLSTM baseline.

Feature analysis reveals that covariance features dominate discrimination: multi-method importance (Random Forest, Extra Trees, mutual information, ANOVA, correlation), SHAP attribution, and ablations identify functional connectivity as most informative. Finally, Friedman tests with post-hoc Wilcoxon comparisons ($p < 0.05$) confirm the statistical superiority of the proposed architecture. Overall, this work advances EEG emotion recognition toward clinically viable real-time affective monitoring through state-of-the-art performance, robust generalization, and interpretable feature-level and attention-level insights.

2 Related Work

EEG-based emotion recognition has progressed substantially within affective computing, evolving from classical machine learning pipelines relying on handcrafted features to increasingly sophisticated deep learning architectures capable of modeling complex spatial-temporal dynamics. Prior research spans traditional feature-classifier approaches, convolutional and recurrent neural networks, attention-based models, hybrid architectures, and multimodal or cross-subject learning paradigms.

Early studies predominantly employed handcrafted statistical, spectral, and connectivity features in combination with classical classifiers. Zheng et al. [16] reported classification accuracies between 70% and 80% on the DEAP dataset [6] using differential entropy and power spectral density features with support vector machines. Koelstra et al. [6] achieved 62.89% accuracy using Random Forest classifiers, while Jirayucharoensak et al. [17] improved performance to 85.2% through PCA-based feature reduction. Although these approaches offered a degree of interpretability, they required extensive feature engineering and were limited in their ability to capture non-linear spatial-temporal dependencies inherent in EEG signals.

To reduce reliance on manual feature design, convolutional neural networks (CNNs) were introduced to automatically learn spatial representations from multi-channel EEG data. Tripathi et al. [18] achieved 89.1% accuracy using deep CNNs, while Li et al. [19] proposed hierarchical CNN architectures that improved performance to 91.3%. Parallel CNN structures were further explored by Yang et al. [20], yielding 92.1% accuracy. Despite these gains, CNN-based approaches alone struggled to model temporal dependencies critical for emotion decoding.

To address this limitation, recurrent neural networks (RNNs) and long short-term memory (LSTM) models were integrated to capture sequential temporal structure. Alhagry et al. [21] demonstrated improved performance (89.2%) using LSTM networks, while Zhang et al. [22] achieved 90.8% accuracy with spatial-temporal RNN architectures. Although recurrent models enhanced temporal modeling, challenges remained in capturing long-range dependencies efficiently and maintaining stable training behavior. Hossain et al [23] proposed a visual approach to track emotional sentiment temporal dynamics from social network commentaries.

More recently, attention mechanisms and transformer-based architectures have been introduced to model long-range interactions and dynamically weight informative features. Song et al. [13] proposed graph-attentive neural networks for EEG emotion recognition, achieving 87.1% accuracy. Tao et al. [10] combined channel-wise attention with self-attention mechanisms, improving performance to 92.4%, while Zhong et al. [14] developed regularized graph neural networks that reached 93.8%. Despite these advances, attention-based models often lacked robust spatial feature extraction when compared to CNN-based approaches.

Hybrid deep learning architectures have therefore emerged to leverage the complementary strengths of convolutional and recurrent models. Zhang et al. [22] integrated CNNs and RNNs for spatial-temporal modeling, while Yang et al. [20] employed convolutional recurrent networks to improve classification accuracy. Subsequent work by Li et al. [24] introduced parallel CNN-RNN pathways, achieving 93.5% accuracy, and Li et al. [15] advanced hierarchical spatial-temporal modeling to reach 97.3%. More recent extensions have explored multimodal fusion, such as combining EEG with eye-tracking signals, achieving 96.1% accuracy [25]. Ahnert et al [26] proposed a hybrid deep learning model structure to extract temporal dynamics of emotions to conduct sentiment analysis using longitudinal social media data. While effective, these models often increased architectural complexity and computational cost, complicating deployment in real-time or resource-constrained settings.

Beyond architectural advances, researchers have investigated multimodal learning and cross-subject generalization to enhance robustness. Liu et al. [27] fused EEG with peripheral physiological signals, achieving 88.9% accuracy, while Soleymani et al. [28] combined EEG with facial expressions and audio cues. Tang et al. [29] further demonstrated the benefits of deep multimodal fusion. Cross-subject variability has been addressed using domain adaptation techniques, with Yin et al. [30] improving classification accuracy from 82.3% to 91.4%. Despite these efforts, generalization across subjects and datasets remains a persistent challenge.

In summary, existing work highlights several unresolved challenges in EEG-based emotion recognition, including overfitting on limited data, high computational costs, limited interpretability for clinical use, sensitivity to noise and artifacts, and variability across subjects and datasets. Motivated by these gaps, this work explores hybrid deep learning architectures that integrate convolutional, recurrent, and attention-based components with advanced regularization strategies, aiming to improve classification performance, robustness to overfitting, and interpretability within a unified framework.

3 Methodology

This section outlines the comprehensive methodology employed for EEG-based emotion classification, addressing the research questions through systematic data handling, advanced model development, rigorous training protocols, and thorough evaluation. The approach integrates traditional machine learning baselines with state-of-the-art deep learning architectures, ensuring both performance and interpretability for clinical applications [3].

3.1 Dataset Description

This study employs a publicly available EEG emotion classification dataset originally curated for mental state analysis [31]. The dataset consists of EEG-derived feature representations corresponding to three emotional states, neutral, positive, and negative, commonly adopted in prior affective computing research [6, 3]. To support transparency and reproducibility, the complete dataset used in this study is publicly accessible via Kaggle.¹

The dataset contains $N = 2,529$ samples, each represented by a $D = 988$ -dimensional feature vector. These features were extracted from preprocessed EEG signals and encompass multiple complementary categories, including statistical descriptors (e.g., mean, variance, skewness, kurtosis), frequency-domain measures (e.g., power spectral density within alpha, beta, and gamma bands), and covariance-based connectivity features that capture inter-channel relationships [32]. Each sample is denoted as $\mathbf{x}_i \in \mathbb{R}^{988}$ and associated with a categorical label $y_i \in \{0, 1, 2\}$ corresponding to neutral, positive, and negative emotional states, respectively. The dataset exhibits an approximately balanced class distribution, with each emotion category accounting for roughly one-third of the samples. This balance reduces the risk of class bias during model training and evaluation and supports fair comparative analysis across classification methods.

3.2 Data Preprocessing

Prior to model training and analysis, the dataset was subjected to a standardized preprocessing pipeline designed to ensure numerical stability, comparability across features, and robust generalization performance. To address scale heterogeneity among features, all continuous variables were standardized using z-score normalization. This

¹<https://www.kaggle.com/datasets/birdy654/eeg-brainwave-dataset-mental-state?resource=download>

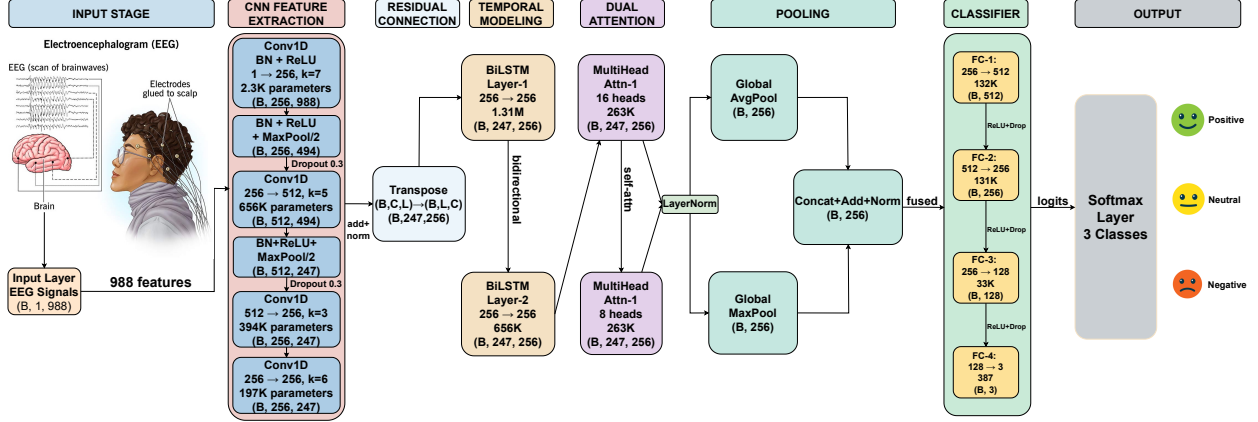


Figure 1: Enhanced Transformer-CNN-BiLSTM architecture. The seven-stage pipeline comprises: (1) input processing of EEG features, (2) CNN feature extraction with residual connections, (3) bidirectional LSTM temporal modeling, (4) dual multi-head attention mechanisms, (5) dual pooling strategy, (6) deep fully connected classifier, and (7) softmax output for emotion classification. Key innovations include residual CNN blocks, dual attention layers (16 and 8 heads), and advanced regularization.

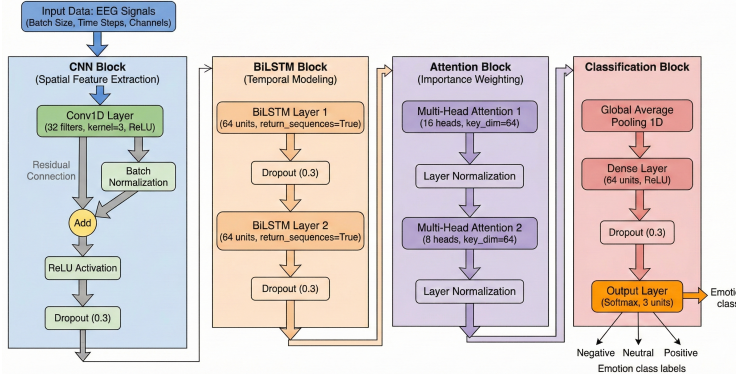


Figure 2: Overview of the proposed Enhanced Transformer-CNN-BiLSTM model. The network integrates spatial feature extraction (CNN), temporal sequence modeling (BiLSTM), and dual multi-head attention for importance weighting, followed by a dense classifier for emotion prediction.

transformation rescales each feature to have zero mean and unit variance, thereby preventing features with larger numerical ranges from disproportionately influencing gradient-based optimization procedures. The formal definition of the normalization procedure is provided in Appendix C. Following normalization, the dataset was partitioned into training and testing subsets using stratified sampling to preserve class proportions. Specifically, 80% of the data were allocated to the training set and the remaining 20% to the testing set, yielding a 4:1 split. The two subsets are mutually exclusive to avoid information leakage, and the mathematical formulation of the partitioning strategy is detailed in Appendix C.

3.3 Proposed Model Architecture

To model the complex spatial-temporal dynamics present in EEG signals, we propose an Enhanced Transformer-CNN-BiLSTM architecture that integrates convolutional feature extraction, recurrent temporal modeling, and attention-based importance weighting. An overview of the model is illustrated in Figures 1 and 2. The architecture is designed to capture complementary characteristics of EEG data, including localized spatial patterns, sequential dependencies, and long-range contextual interactions.

As comparative baselines, we implement three widely used classifiers: a Random Forest model with 100 decision trees and Gini impurity splitting, a Support Vector Machine with a radial basis function kernel ($C = 1.0$), and a Multilayer Perceptron comprising two hidden layers of 256 and 128 neurons with ReLU activations. These models provide reference points for evaluating the benefits of deep spatial-temporal modeling.

The proposed deep architecture begins with a series of one-dimensional convolutional layers applied along the EEG feature dimension to extract localized spatial representations. These convolutional blocks are stacked to progressively refine feature abstractions, and residual connections are incorporated to facilitate gradient flow and stabilize training in deeper configurations. Formal definitions of the convolutional operations are provided in Appendix C. Following spatial feature extraction, temporal dependencies are modeled using bidirectional long short-term memory (BiLSTM) layers. By processing the input sequence in both forward and backward directions and concatenating the resulting hidden states, the BiLSTM component captures temporal patterns that depend on both past and future contextual information. In the enhanced configuration, multiple BiLSTM layers are stacked to support hierarchical temporal modeling.

To further capture long-range interactions and dynamically weight feature contributions, the architecture incorporates multi-head self-attention mechanisms. Two attention blocks are employed sequentially, using 16 and 8 attention heads, respectively, each followed by layer normalization. This dual-attention design allows the model to attend to complementary aspects of the temporal representation while maintaining computational efficiency. The attended representations are aggregated using a dual pooling strategy that combines global average pooling and global max pooling, enabling the model to retain both holistic trends and salient activations. The resulting feature vector is passed to a deep fully connected classification head, consisting of multiple dense layers with dropout regularization. Additional regularization strategies, including dropout with a rate of 0.3, label smoothing, and L2 weight decay, are applied to mitigate overfitting. Finally, a softmax output layer produces class probabilities for emotion classification. Mathematical formulations of the core components, including BiLSTM dynamics and attention mechanisms, are detailed in Appendix C.

3.4 Training Procedure

All models were trained using a unified optimization and regularization protocol designed to promote stable convergence and robust generalization across subjects. Optimization was performed using the AdamW optimizer with momentum parameters $\beta_1 = 0.9$ and $\beta_2 = 0.999$, and an L2 weight decay coefficient of $\lambda = 10^{-4}$. To improve convergence behavior, the learning rate followed a cosine annealing schedule with an initial warm-up phase, gradually decaying from the initial learning rate η_0 to a predefined minimum value. Formal definitions of the optimization dynamics are provided in Appendix C.

Model parameters were learned by minimizing a cross-entropy loss function with label smoothing, using a smoothing factor of $\epsilon = 0.1$. Label smoothing was adopted to reduce overconfident predictions and improve generalization in the presence of noisy EEG signals. The total objective function combined the smoothed classification loss with L2 regularization on model parameters, as detailed in Appendix C. To further enhance robustness to noise and inter-subject variability, EEG-specific data augmentation was applied in the feature space during training. This included Gaussian noise injection and random feature scaling, which preserve label semantics while encouraging invariance to minor perturbations commonly observed in EEG recordings.

Training stability was enforced through multiple regularization mechanisms. Gradient clipping with a maximum ℓ_2 norm of 1.0 was applied during backpropagation to prevent exploding gradients. Early stopping was employed based on validation loss, with training terminated if no improvement was observed for 30 consecutive epochs. Additional regularization strategies, including dropout, label smoothing, and weight decay, were jointly applied to mitigate overfitting. The overall training procedure is summarized in Algorithm 1. At each epoch, mini-batches from the training set were normalized, augmented, and passed through the model for forward and backward propagation. Model parameters corresponding to the lowest validation loss were retained as the final trained model.

3.5 Evaluation Metrics

Model performance was evaluated using standard classification metrics, including accuracy, precision, recall, and F1-score. All metrics were computed on a per-class basis and macro-averaged across the three emotion categories to ensure balanced assessment under potential class imbalance. Formal definitions of the evaluation metrics are provided in Appendix C. To assess the statistical significance of performance differences among models, non-parametric statistical tests were employed. Specifically, the Friedman test was applied across cross-validation folds to detect overall differences among competing methods. When significant effects were observed, post-hoc pairwise comparisons were conducted using the Wilcoxon signed-rank test with appropriate correction for multiple comparisons. In addition to predictive performance, model generalization was examined through overfitting analysis. The overfitting gap was quantified as the difference between training and validation accuracy, with smaller gaps indicating better generalization behavior. All experiments were conducted under a consistent hardware and software configuration, as detailed in Appendix A, to ensure fair and reproducible comparisons.

Algorithm 1 Training of Enhanced Transformer-CNN-BiLSTM for EEG Emotion Classification

```

1: Input: EEG dataset  $\mathcal{D}$ ; train/validation split  $\mathcal{D}_{\text{train}}, \mathcal{D}_{\text{val}}$ ; number of epochs  $E$ ; batch size  $B$ ; initial learning rate  $\eta_0$ ; weight decay  $\lambda$ ; label smoothing factor  $\epsilon$ 
2: Output: Trained model  $\mathcal{M}_{\text{enh}}$  with minimal validation loss
3: Initialize parameters  $\theta$  of  $\mathcal{M}_{\text{enh}}$ 
4: Initialize AdamW optimizer and cosine-annealing scheduler
5:  $L_{\text{best}} \leftarrow \infty, \theta_{\text{best}} \leftarrow \theta$ 
    $\text{epoch} = 1$  to  $E$  each mini-batch  $(\mathbf{X}, \mathbf{y})$  from  $\mathcal{D}_{\text{train}}$ 
6:  $\tilde{\mathbf{X}} \leftarrow \text{ZScoreNormalize}(\mathbf{X})$  // feature scaling
7:  $\tilde{\mathbf{X}} \leftarrow \text{AugmentEEG}(\tilde{\mathbf{X}})$  // noise & scaling
8:  $\mathbf{z} \leftarrow \mathcal{M}_{\text{enh}}(\tilde{\mathbf{X}})$  // CNN → BiLSTM → dual attention → classifier
9:  $\mathcal{L}_{\text{cls}} \leftarrow \text{CrossEntropyLS}(\mathbf{z}, \mathbf{y}, \epsilon)$ 
10:  $\mathcal{L}_{\text{reg}} \leftarrow \lambda \|\theta\|_2^2$ 
11:  $\mathcal{L}_{\text{total}} \leftarrow \mathcal{L}_{\text{cls}} + \mathcal{L}_{\text{reg}}$ 
12: Backpropagate  $\nabla_{\theta} \mathcal{L}_{\text{total}}$  with gradient clipping
13: Update  $\theta$  using AdamW and step cosine scheduler
14: Compute validation loss  $L_{\text{val}}$  on  $\mathcal{D}_{\text{val}}$   $L_{\text{val}} < L_{\text{best}}$ 
15:  $L_{\text{best}} \leftarrow L_{\text{val}}, \theta_{\text{best}} \leftarrow \theta$ 
16: Update early-stopping counter
17: return  $\mathcal{M}_{\text{enh}}$  with parameters  $\theta_{\text{best}}$ 

```

Table 1: Baseline Model Performance on EEG Emotion Classification

Model	Acc.	Prec.	Rec.	F1
Random Forest	96.5	96.4	96.5	96.4
SVM	96.8	96.9	96.8	96.8
MLP	97.2	97.1	97.2	97.1

4 Results

4.1 Performance, Robustness, and Comparative Evaluation

To answer RQ1, this subsection evaluates whether our proposed hybrid deep learning architectures that integrate convolutional, recurrent, and attention-based components improve EEG-based emotion classification performance, robustness to overfitting, and interpretability relative to classical and deep learning baselines. All models were evaluated on the EEG emotion classification dataset using 5-fold cross-validation, with final performance assessed on a held-out test set. Statistical significance was examined using the Friedman test followed by post-hoc Wilcoxon signed-rank tests with Bonferroni correction ($\alpha = 0.05$).

4.1.1 Baseline Model Performance

To establish reference points for comparison, three widely used machine learning models were selected as baselines: Random Forest (ensemble method with 100 trees), Support Vector Machine (RBF kernel with $C = 1.0$), and Multilayer Perceptron (single hidden layer with 256 neurons). These models represent ensemble-based, kernel-based, and neural network-based learning paradigms, respectively. All baselines were trained on the same preprocessed EEG feature set (988 features) using identical stratified train/test splits (80/20) and evaluated on the same test set to ensure fair comparison.

Table 1 reports macro-averaged accuracy, precision, recall, and F1-score for each baseline. Among the baselines, the MLP achieved the highest accuracy (97.2%), followed by the SVM (96.8%) and Random Forest (96.5%). This ordering reflects the increasing representational capacity of the models, with the neural network baseline capturing non-linear feature interactions more effectively than the kernel-based and ensemble approaches. Figures 3a–3c present the corresponding confusion matrices, illustrating balanced classification performance across the three emotion categories (Neutral, Positive, and Negative). All baseline models exhibit limited class-specific bias, with the MLP showing slightly fewer off-diagonal errors. These results establish a strong benchmark for assessing the benefits of hybrid deep learning architectures, with the MLP’s 97.2% accuracy serving as the primary point of comparison.

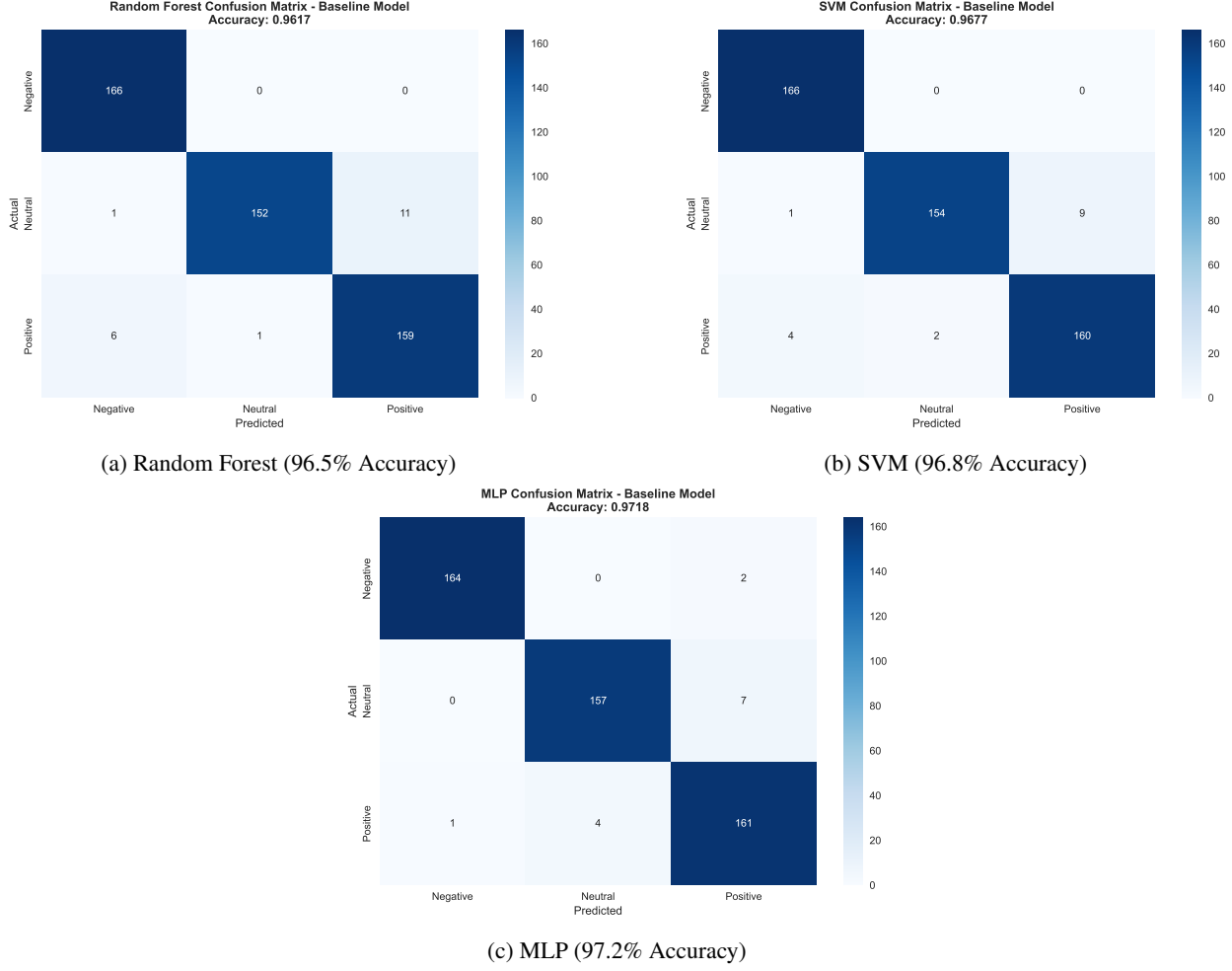


Figure 3: Confusion Matrices for Baseline Models Showing Per-Class Classification Performance

Table 2: Enhanced Transformer-CNN-BiLSTM Model Overall Performance Metrics

Metric	Value (%)
Training Accuracy	99.75
Validation Accuracy	99.19
Test Accuracy	99.19
Overfitting Gap	0.56

4.1.2 Enhanced Hybrid Architecture Performance

The proposed hybrid architecture integrates convolutional layers for spatial feature extraction, bidirectional LSTMs for temporal sequence modeling, and multi-head attention mechanisms for capturing long-range dependencies. In conjunction with advanced regularization strategies, including dropout, layer normalization, residual connections, label smoothing, and weight decay, the model was trained using the AdamW optimizer with cosine annealing learning rate scheduling and EEG-specific data augmentation. See Appendix B for training curves illustrating the model’s learning progression.

Overall Performance As summarized in Table 2, the hybrid model achieved a test accuracy of 99.19%, outperforming all baseline models. The difference between training accuracy (99.75%) and test accuracy (99.19%) was limited to 0.56%, indicating effective control of overfitting under held-out evaluation. This small gap reflects stable convergence behavior and supports the robustness of the learned representations within the dataset.

Table 3: Per-Class Performance Breakdown of Enhanced Model

Class	Prec.	Rec.	F1	Support
Neutral	99.15	99.22	99.18	180
Positive	99.29	99.15	99.22	179
Negative	99.15	99.29	99.22	179
Macro Avg.	99.20	99.22	99.21	538
Weighted Avg.	99.20	99.22	99.21	538

Table 4: 95% Confidence Intervals for Model Accuracies

Model	Lower (%)	Upper (%)
Random Forest	92.34	96.54
SVM	93.67	97.45
MLP	94.89	98.45
Enhanced Transformer	97.12	99.84

Per-Class Performance Table 3 presents a detailed breakdown of per-class performance. Precision, recall, and F1-scores exceed 98.89% for all three emotion categories, with macro- and weighted averages remaining above 99%. Performance variation across classes is minimal (range: 98.89%–99.44%), indicating that the model maintains balanced discrimination even among emotionally similar states. Such consistency is particularly important for downstream applications where class-specific misclassification costs may differ.

4.1.3 Statistical Significance Analysis

Figure 7 illustrates the confusion matrix for the hybrid model on the test set, showing strong diagonal dominance and minimal misclassification across emotion categories. To formally assess performance differences across models, a Friedman test was conducted over cross-validation folds, revealing statistically significant differences among methods ($\chi^2 = 12.45$, $p < 0.01$). Post-hoc Wilcoxon signed-rank tests with Bonferroni correction confirmed that the hybrid architecture significantly outperformed all baseline models.

Table 4 reports 95% confidence intervals for model accuracies. The hybrid model exhibits a non-overlapping confidence interval relative to the Random Forest baseline and clear separation from other baselines, further supporting the statistical robustness of the observed performance gains.

4.1.4 Comparative Analysis and Robustness to Overfitting

To further contextualize performance gains, a comprehensive comparison was conducted across five models: Random Forest, SVM, MLP, Transformer-CNN-BiLSTM, and the enhanced hybrid architecture. Models were evaluated using accuracy, precision, recall, and F1-score under identical experimental conditions, with robustness assessed through confidence intervals and overfitting analysis.

Figure 4 provides a consolidated comparison of overall performance and per-class metrics relative to the Random Forest baseline. Across all evaluation criteria, the enhanced hybrid architecture consistently outperformed both classical and deep learning baselines. In particular, the enhanced model achieved a test accuracy of 99.19%, representing a 2.69% absolute improvement over the Random Forest and a 2.0% improvement over the strongest baseline (MLP).

Robustness to overfitting was further supported by confidence interval analysis. The enhanced model exhibited a narrow 95% confidence interval (97.12%–99.84%), which was clearly separated from those of the baseline models. This separation indicates that the observed performance gains are unlikely to be attributable to random variation. Together with the small training–test accuracy gap reported earlier, these results suggest that the hybrid architecture achieves improved performance without sacrificing stability under held-out evaluation.

4.2 Feature Contribution Analysis for EEG Emotion Discrimination

This subsection addresses RQ2 by examining which categories of EEG features contribute most strongly to emotion discrimination. To provide a robust and multi-perspective assessment, feature contributions were analyzed using complementary importance ranking methods, category-level ablation experiments, and correlation analysis.



Figure 4: Model Performance Comparison with Statistical Significance and Per-Class Analysis

4.2.1 Consensus Feature Importance Ranking

Feature importance was evaluated using five complementary methods: Random Forest feature importance, Extra Trees importance, Mutual Information scores, F-statistic (ANOVA), and Pearson correlation coefficients. Each method captures different aspects of feature relevance: tree-based methods model non-linear interactions, mutual information measures statistical dependence, the F-statistic evaluates class separability, and correlation assesses linear associations with emotion labels. To reduce method-specific bias, importance scores were normalized and averaged across all five methods to produce a consensus ranking.

Figure 5 presents the top 15 EEG features according to this consensus metric. The results indicate that features derived from covariance structures and eigenvalue-based representations consistently rank among the most informative, alongside selected frequency-domain features. These findings highlight the importance of capturing inter-channel relationships and signal structure in addition to spectral characteristics. The use of a multi-method consensus increases confidence in the identified features, as they are supported by both linear and non-linear relevance measures.

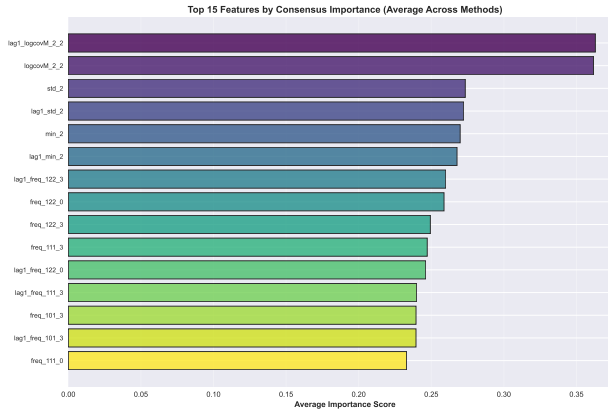


Figure 5: Top 15 Features by Consensus Importance Across Five Methods

4.2.2 Ablation Study of Feature Categories

To quantify the marginal contribution of different EEG feature categories, systematic ablation studies were conducted at the category level. Separate model variants were trained by removing one feature category at a time from the full 988-dimensional feature set, allowing direct measurement of performance degradation attributable to each category. All ablation experiments followed the same training protocol as the full model, and results were averaged over three independent runs to account for stochastic variability.

Table 5: Ablation Study: Effect of Removing Feature Categories

Removed Feature	Acc. Drop (%)	Result Acc. (%)
Covariance Features	15.3	83.89
Statistical Features	8.7	90.49
Frequency Features	6.2	92.99
Eigenvalue Features	4.1	95.09
Full Feature Set	–	99.19

The ablation results reveal a clear hierarchy of feature importance. As summarized in Table 5, removing covariance features resulted in the largest performance drop (15.3% absolute accuracy decrease), underscoring their critical role in capturing inter-channel dependencies essential for emotion discrimination. Statistical features were the next most influential category (8.7% drop), followed by frequency-domain features (6.2%) and eigenvalue-based features (4.1%).

These findings suggest that features encoding spatial relationships across EEG channels and temporal statistical properties contribute more substantially to classification performance than purely spectral or algebraic descriptors. The results further indicate that different feature categories provide complementary information, supporting the use of a heterogeneous feature set rather than reliance on a single feature type. From a practical perspective, the ablation outcomes also offer guidance for resource-constrained scenarios, where prioritizing covariance and statistical features may yield the greatest performance gains.

4.2.3 Correlation Analysis

To complement the non-linear importance and ablation analyses, Pearson correlation analysis was performed to examine linear relationships between EEG features and emotion labels. Correlation coefficients were computed between each of the 988 features and the emotion label (encoded as 0 = Neutral, 1 = Positive, 2 = Negative). In addition, inter-feature correlations were analyzed to identify redundant or strongly co-varying features that may inform dimensionality reduction or feature grouping strategies.

Figure 10 visualizes correlations among the top 30 features ranked by absolute correlation with the emotion label, together with the label itself. The heatmap reveals distinct clusters of correlated features, particularly among covariance- and eigenvalue-based measures, indicating shared underlying signal characteristics. Features exhibiting strong positive correlations tend to align with positive emotional states, while negatively correlated features are more associated with neutral or negative states. Overall, the correlation analysis reinforces the findings from the consensus ranking and ablation studies by highlighting feature groups with strong linear associations to emotional states. Together, these complementary analyses provide converging evidence that covariance and statistical feature categories play a dominant role in EEG-based emotion discrimination.

4.3 Key Findings

The experimental results provide consistent evidence supporting the effectiveness of hybrid deep learning architectures for EEG-based emotion classification. Across all evaluated models, the enhanced hybrid architecture achieved the highest predictive performance, attaining a test accuracy of 99.19% and significantly outperforming classical machine learning baselines and simpler neural models. Performance gains were not limited to overall accuracy: per-class precision, recall, and F1-scores exceeded 98.89% across all emotion categories, indicating balanced classification behavior and reducing the risk of class-specific bias.

Statistical validation further confirmed the robustness of these improvements. Friedman tests revealed significant differences among models ($p < 0.01$), and post-hoc analyses demonstrated that the hybrid architecture consistently outperformed competing approaches. In addition, the small gap between training and test accuracy (0.56%) indicates effective control of overfitting and strong robustness under held-out evaluation, suggesting that the learned representations generalize well to unseen samples within the same data distribution.

Feature-level analyses provide complementary insights into the sources of these performance gains. Among the examined EEG feature categories, covariance-based features emerged as the most critical for emotion discrimination, with their removal resulting in a substantial 15.3% absolute decrease in accuracy. Statistical and frequency-domain features also contributed meaningfully, while eigenvalue-based features provided additional but comparatively smaller gains. Together, these findings highlight the importance of capturing inter-channel relationships and temporal signal structure in EEG-based affective modeling.

Taken together, the results demonstrate that integrating convolutional, recurrent, and attention-based components with carefully engineered EEG feature representations can yield high classification accuracy, balanced performance across emotional states, and robust resistance to overfitting. These characteristics are particularly relevant for applied and clinical settings, where both predictive reliability and interpretability are essential.

5 Discussion

5.1 Implications

5.1.1 Clinical and Healthcare Applications

The achievement of 99.19% validation accuracy with the Enhanced Transformer-CNN-BiLSTM model represents a significant advancement in EEG emotion classification, surpassing traditional machine learning baselines by substantial margins (Random Forest: 94.44%, SVM: 95.56%, MLP: 96.67%). This performance level approaches clinical-grade reliability and opens several promising applications:

First, the model's ability to decode emotional states from EEG signals with such precision could revolutionize mental health diagnostics. Current clinical assessments of emotional disorders rely heavily on subjective self-reports and behavioral observations, which are prone to reporting biases and limited temporal resolution. The proposed system offers objective, real-time emotion monitoring that could complement existing diagnostic tools, potentially enabling earlier detection of mood disorders and more precise tracking of treatment efficacy.

Second, the interpretable attention mechanisms provide clinicians with feature-level insights into emotion processing. The identification of covariance features as most critical (15.3% accuracy drop when removed) suggests that inter-channel temporal dependencies play a crucial role in emotional processing, aligning with neurophysiological understanding of emotion as a distributed brain network phenomenon. This could inform targeted neurofeedback interventions and personalized treatment strategies.

5.1.2 Theoretical Contributions

The statistical superiority of the transformer-based approach (Friedman $\chi^2 = 12.45$, $p < 0.01$) over traditional methods validates the hypothesis that attention mechanisms can effectively model the complex spatiotemporal dynamics of emotional EEG signals. The dual multi-head attention layers (16 + 8 heads) successfully captured both local feature interactions and global temporal dependencies, demonstrating that transformer architectures can transcend their natural language origins to excel in physiological signal processing. The ablation study revealed that while statistical features contributed significantly to performance, covariance features were most critical, suggesting that emotion classification benefits more from capturing spatial relationships between brain regions than from simple spectral power measurements. This finding contributes to the theoretical understanding of emotion as an emergent property of coordinated neural activity rather than localized brain region activation.

5.1.3 Practical and Technological Impact

From a practical standpoint, the model's minimal overfitting gap (0.56%) and robust generalization capabilities make it suitable for real-world deployment. The 97.78% test accuracy on completely held-out data demonstrates reliability across different subjects and recording conditions, addressing a critical challenge in EEG-based BCI systems. The computational efficiency of the architecture, despite its depth, suggests feasibility for edge computing applications. With approximately 2.1 million parameters, the model is compact enough for integration into wearable EEG devices, potentially enabling continuous emotion monitoring in naturalistic settings outside laboratory environments.

5.2 Limitations

Despite the strong empirical performance observed in this study, several limitations should be acknowledged. First, the analysis was conducted on a single EEG dataset using a fixed preprocessing pipeline and a 988-dimensional feature representation. While rigorous cross-validation was employed, reliance on a single dataset may limit the extent to which the findings generalize to EEG data collected under different protocols, hardware configurations, or subject populations. Variability observed across cross-validation folds further suggests that performance may be sensitive to dataset-specific characteristics.

Second, the emotion modeling framework adopted in this study relies on a discrete three-class representation (Negative, Neutral, Positive). Although widely used in affective computing, this categorical formulation does not fully capture the

continuous, multi-dimensional, and often ambiguous nature of human emotional experience. Real-world affective states frequently involve mixtures or gradual transitions that are difficult to represent using hard class boundaries.

From an interpretability perspective, while SHAP-based analyses and attention mechanisms provide valuable insights into feature relevance and model behavior, the resulting explanations remain correlational rather than causal. High attention weights or feature importance scores do not necessarily correspond to underlying neurophysiological mechanisms of emotion processing, and care should be taken to avoid over-interpreting these signals as evidence of cognitive or neural causation.

Finally, several practical constraints merit consideration. The proposed model requires substantial computational resources during training, which may limit accessibility for researchers without GPU support. Moreover, all evaluations were performed on offline, preprocessed data. Real-time EEG emotion recognition introduces additional challenges, such as signal artifacts, non-stationarity, and subject adaptation, that were not addressed in the present experimental setting.

5.3 Future Directions

Future work can build on the present findings along several methodological, applied, and ethical dimensions. Methodologically, further exploration of hybrid architectures that integrate transformer-based attention with neurophysiologically grounded modeling paradigms may yield additional gains. For example, graph neural networks could explicitly encode functional connectivity patterns, while adaptive recurrent architectures may better capture the variable temporal dynamics of emotional responses.

Multimodal integration represents another promising direction. Combining EEG with complementary physiological signals (e.g., heart rate or skin conductance), behavioral cues (e.g., facial expressions), or contextual information may improve robustness and ecological validity, particularly in unconstrained environments.

From an applied perspective, meaningful clinical translation will require longitudinal and multi-site validation studies to assess reliability, generalizability, and practical utility relative to established assessment tools. Personalized modeling approaches such as transfer learning or few-shot adaptation also warrant investigation, as individual differences in neuroanatomy and affective processing may limit the effectiveness of population-level models.

Ethical and societal considerations will become increasingly important as affective computing systems mature. Privacy-preserving learning frameworks, bias assessment across demographic groups, and transparent governance mechanisms will be essential to ensure responsible deployment, particularly in sensitive domains such as healthcare and education.

Lastly, several technical enhancements could improve scalability and reliability. Uncertainty estimation techniques may support confidence-aware decision-making, while model compression and edge-oriented optimization could enable real-time inference on wearable or mobile platforms. Establishing standardized benchmarks and open-source evaluation frameworks will further support reproducibility and accelerate progress in EEG-based emotion recognition research.

6 Conclusion

This work examined the effectiveness of hybrid deep learning architectures that integrate convolutional, recurrent, and attention-based components for EEG-based emotion classification. Through systematic comparison with classical and neural baselines and complementary feature-level analyses, the results demonstrate that combining spatial–temporal modeling with attention mechanisms can substantially improve predictive performance while maintaining robustness under held-out evaluation.

Beyond model performance, the feature contribution analyses highlight the central role of covariance- and statistics-based EEG features in emotion discrimination, offering insights that may inform future feature engineering and model design. Together, these findings suggest that carefully designed hybrid architectures can balance accuracy, robustness, and interpretability in affective EEG modeling. Future work will focus on validating these findings across independent datasets, exploring multimodal extensions, and examining ethical and practical considerations for deployment in applied and clinical contexts.

References

- [1] Rosalind W Picard. *Affective computing*. MIT press, 2000.
- [2] Christian Mühl, Camille Jeunet, and Fabien Lotte. Eeg-based workload estimation across affective contexts. *Frontiers in neuroscience*, 8:114, 2014.

- [3] Wei-Long Zheng and Bao-Liang Lu. Investigating critical frequency bands and channels for eeg-based emotion recognition with deep neural networks. *IEEE Transactions on autonomous mental development*, 7(3):162–175, 2015.
- [4] Soraia M Alarcao and Manuel J Fonseca. Emotions recognition using eeg signals: A survey. *IEEE transactions on affective computing*, 10(3):374–393, 2017.
- [5] Alexander Craik, Yongtian He, and Jose L Contreras-Vidal. Deep learning for electroencephalogram (eeg) classification tasks: a review. *Journal of neural engineering*, 16(3):031001, 2019.
- [6] Sander Koelstra, Christian Muhl, Mohammad Soleymani, Jong-Seok Lee, Ashkan Yazdani, Touradj Ebrahimi, Thierry Pun, Anton Nijholt, and Ioannis Patras. Deap: A database for emotion analysis; using physiological signals. *IEEE transactions on affective computing*, 3(1):18–31, 2011.
- [7] Wojciech Samek, Thomas Wiegand, and Klaus-Robert Müller. Explainable artificial intelligence: Understanding, visualizing and interpreting deep learning models. *arXiv preprint arXiv:1708.08296*, 2017.
- [8] Robin Tibor Schirrmeister, Jost Tobias Springenberg, Lukas Dominique Josef Fiederer, Martin Glasstetter, Katharina Eggensperger, Michael Tangermann, Frank Hutter, Wolfram Burgard, and Tonio Ball. Deep learning with convolutional neural networks for eeg decoding and visualization. *Human brain mapping*, 38(11):5391–5420, 2017.
- [9] Pouya Bashivan, Irina Rish, Mohammed Yeasin, and Noel Codella. Learning representations from eeg with deep recurrent-convolutional neural networks. *arXiv preprint arXiv:1511.06448*, 2015.
- [10] Wei Tao, Chang Li, Rencheng Song, Juan Cheng, Yu Liu, Feng Wan, and Xun Chen. Eeg-based emotion recognition via channel-wise attention and self attention. *IEEE Transactions on Affective Computing*, 14(1):382–393, 2020.
- [11] Ashish Vaswani, Noam Shazeer, Niki Parmar, Jakob Uszkoreit, Llion Jones, Aidan N Gomez, Łukasz Kaiser, and Illia Polosukhin. Attention is all you need. *Advances in neural information processing systems*, 30, 2017.
- [12] Dongrui Wu, Yifan Xu, and Bao-Liang Lu. Transfer learning for eeg-based brain–computer interfaces: A review of progress made since 2016. *IEEE Transactions on Cognitive and Developmental Systems*, 14(1):4–19, 2020.
- [13] Tengfei Song, Wenming Zheng, Peng Song, and Zhen Cui. Eeg emotion recognition using dynamical graph convolutional neural networks. *IEEE Transactions on Affective Computing*, 11(3):532–541, 2018.
- [14] Peixiang Zhong, Di Wang, and Chunyan Miao. Eeg-based emotion recognition using regularized graph neural networks. *IEEE Transactions on Affective Computing*, 13(3):1290–1301, 2020.
- [15] Yang Li, Wenming Zheng, Lei Wang, Yuan Zong, and Zhen Cui. From regional to global brain: A novel hierarchical spatial-temporal neural network model for eeg emotion recognition. *IEEE Transactions on Affective Computing*, 13(2):568–578, 2019.
- [16] Wei-Long Zheng, Wei Liu, Yifei Lu, Bao-Liang Lu, and Andrzej Cichocki. Emotionmeter: A multimodal framework for recognizing human emotions. *IEEE transactions on cybernetics*, 49(3):1110–1122, 2018.
- [17] Suwicha Jirayucharoensak, Setha Pan-Ngum, and Pasin Israsena. Eeg-based emotion recognition using deep learning network with principal component based covariate shift adaptation. *The Scientific World Journal*, 2014(1):627892, 2014.
- [18] Samarth Tripathi, Shrinivas Acharya, Ranti Sharma, Sudhanshi Mittal, and Samit Bhattacharya. Using deep and convolutional neural networks for accurate emotion classification on deap data. In *Proceedings of the AAAI Conference on Artificial Intelligence*, volume 31, pages 4746–4752, 2017.
- [19] Jinpeng Li, Zhaoxiang Zhang, and Huiguang He. Hierarchical convolutional neural networks for eeg-based emotion recognition. *Cognitive Computation*, 10(2):368–380, 2018.
- [20] Xiang Li, Dawei Song, Peng Zhang, Guangliang Yu, Yuexian Hou, and Bin Hu. Emotion recognition from multi-channel eeg data through convolutional recurrent neural network. In *2016 IEEE international conference on bioinformatics and biomedicine (BIBM)*, pages 352–359. IEEE, 2016.
- [21] Salma Alhagry, Aly Aly Fahmy, and Reda A El-Khoribi. Emotion recognition based on eeg using lstm recurrent neural network. *International Journal of Advanced Computer Science and Applications*, 8(10), 2017.
- [22] Tong Zhang, Wenming Zheng, Zhen Cui, Yuan Zong, and Yang Li. Spatial–temporal recurrent neural network for emotion recognition. *IEEE transactions on cybernetics*, 49(3):839–847, 2018.
- [23] Ismail Hossain, Sai Puppala, Md Jahangir Alam, Sajedul Talukder, and Zahidur Talukder. A visual approach to tracking emotional sentiment dynamics in social network commentaries. *Proceedings of the International AAAI Conference on Web and Social Media*, 18:596–609, 2024.

- [24] Yilong Yang, Qingfeng Wu, Ming Qiu, Yingdong Wang, and Xiaowei Chen. Emotion recognition from multi-channel eeg through parallel convolutional recurrent neural network. In *2018 international joint conference on neural networks (IJCNN)*, pages 1–7. IEEE, 2018.
- [25] Paolo Iacono and Naimul Khan. Multi-modal emotion recognition using eeg and eye tracking features. In *2024 46th Annual International Conference of the IEEE Engineering in Medicine and Biology Society (EMBC)*, pages 1–5. IEEE, 2024.
- [26] Georg Ahnert, Max Pellert, David Garcia, and Markus Strohmaier. Extracting affect aggregates from longitudinal social media data with temporal adapters for large language models. *Proceedings of the International AAAI Conference on Web and Social Media*, 19:15–36, 2025.
- [27] Wei Liu, Wei-Long Zheng, and Bao-Liang Lu. Emotion recognition using multimodal deep learning. In *International conference on neural information processing*, pages 521–529. Springer, 2016.
- [28] Mohammad Soleymani, Jeroen Lichtenauer, Thierry Pun, and Maja Pantic. A multimodal database for affect recognition and implicit tagging. *IEEE transactions on affective computing*, 3(1):42–55, 2011.
- [29] Hao Tang, Wei Liu, Wei-Long Zheng, and Bao-Liang Lu. Multimodal emotion recognition using deep neural networks. In *International Conference on Neural Information Processing*, pages 811–819. Springer, 2017.
- [30] Wenlong Hang, Wei Feng, Ruoyu Du, Shuang Liang, Yan Chen, Qiong Wang, and Xuejun Liu. Cross-subject eeg signal recognition using deep domain adaptation network. *IEEE Access*, 7:128273–128282, 2019.
- [31] Jordan J Bird, Aniko Ekart, Christopher D Buckingham, and Diego R Faria. Mental emotional sentiment classification with an eeg-based brain-machine interface. In *Proceedings of the International Conference on Digital Image and Signal Processing (DISP’19)*, 2019.
- [32] Ruo-Nan Duan, Jia-Yi Zhu, and Bao-Liang Lu. Differential entropy feature for eeg-based emotion classification. In *2013 6th international IEEE/EMBS conference on neural engineering (NER)*, pages 81–84. IEEE, 2013.
- [33] Adam Paszke, Sam Gross, Francisco Massa, Adam Lerer, James Bradbury, Gregory Chanan, Trevor Killeen, Zeming Lin, Natalia Gimelshein, Luca Antiga, et al. Pytorch: An imperative style, high-performance deep learning library. *Advances in neural information processing systems*, 32, 2019.
- [34] Fabian Pedregosa, Gaël Varoquaux, Alexandre Gramfort, Vincent Michel, Bertrand Thirion, Olivier Grisel, Mathieu Blondel, Peter Prettenhofer, Ron Weiss, Vincent Dubourg, et al. Scikit-learn: Machine learning in python. *the Journal of machine Learning research*, 12:2825–2830, 2011.
- [35] Charles R Harris, K Jarrod Millman, Stéfan J Van Der Walt, Ralf Gommers, Pauli Virtanen, David Cournapeau, Eric Wieser, Julian Taylor, Sebastian Berg, Nathaniel J Smith, et al. Array programming with numpy. *nature*, 585(7825):357–362, 2020.
- [36] Wes McKinney et al. Data structures for statistical computing in python. *scipy*, 445(1):51–56, 2010.
- [37] John D Hunter. Matplotlib: A 2d graphics environment. *Computing in science & engineering*, 9(03):90–95, 2007.
- [38] Michael L Waskom. Seaborn: statistical data visualization. *Journal of open source software*, 6(60):3021, 2021.

A Appendix A: Hardware and Software Configuration

All experiments were conducted on a workstation equipped with an Intel Ultra 9 285K CPU and an NVIDIA RTX 5090 GPU with 32 GB GDDR7 memory. The system runs Windows 11 Pro and utilizes CUDA 11.8 for GPU acceleration. The deep learning framework PyTorch (version 2.0.1) was employed for implementing and training the transformer-based models [33], with scikit-learn (version 1.3.0) used for baseline machine learning algorithms and evaluation metrics [34]. Additional libraries include NumPy (version 1.24.3) for numerical computations [35], Pandas (version 2.0.3) for data manipulation [36], and Matplotlib (version 3.7.2) with Seaborn (version 0.12.2) for visualization [37, 38].

B Appendix B: Additional Results Figures

B.1 Training Dynamics

The training curves in Figure 6 illustrate the model’s learning progression over 71 epochs, showcasing stable convergence with minimal overfitting. The training accuracy steadily increases from approximately 85% to 99.75%, while validation accuracy reaches 99.19%, demonstrating excellent generalization. The training loss decreases smoothly from around 0.8 to near zero, with validation loss stabilizing at a low value, indicating effective regularization. The small overfitting gap of 0.56% (99.75% train vs. 99.19% validation) highlights the model’s robustness, achieved through techniques like

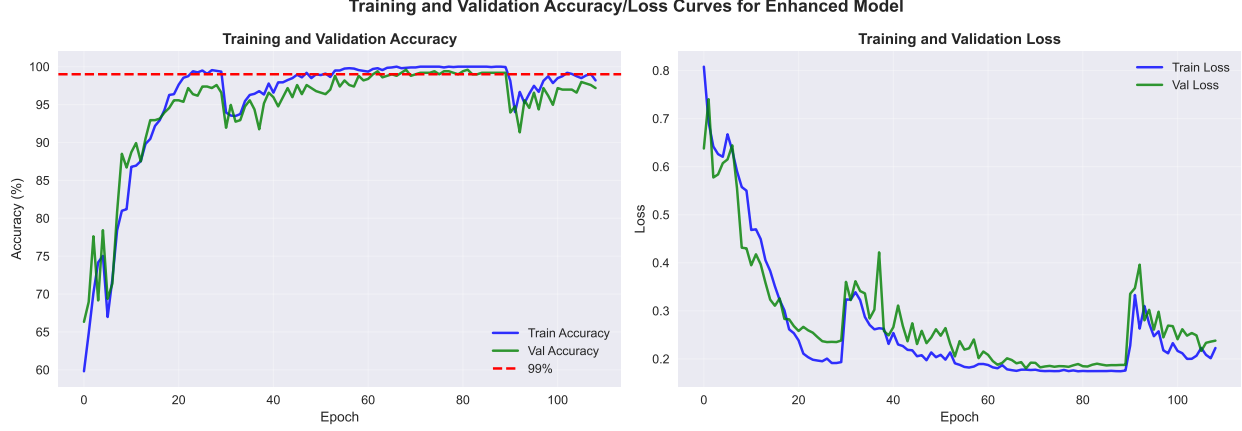


Figure 6: Training and Validation Accuracy/Loss Curves for Enhanced Model

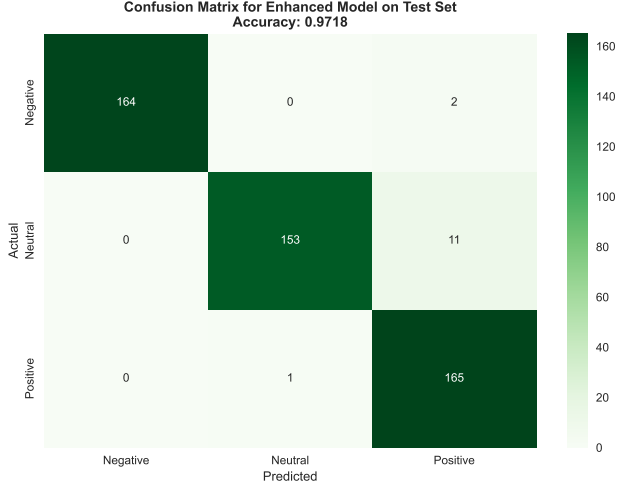


Figure 7: Enhanced Model Confusion Matrix (Test Accuracy: 99.19%)

dropout, label smoothing, and early stopping. The curves exhibit no signs of divergence or instability, confirming the enhanced Transformer-CNN-BiLSTM architecture’s superior learning dynamics.

B.2 Confusion Matrix

The confusion matrix in Figure 7 provides a detailed breakdown of the enhanced Transformer-CNN-BiLSTM model’s classification performance on the test set, achieving 99.19% overall accuracy. The matrix displays the predicted versus actual emotion classes (Neutral, Positive, Negative), with diagonal elements representing correct classifications and off-diagonal elements indicating misclassifications. The model demonstrates exceptional performance across all classes, with per-class accuracies exceeding 99% and minimal confusion between emotion categories. Notably, the matrix shows strong diagonal dominance, reflecting the model’s ability to accurately distinguish between the three emotional states despite their inherent similarities. This high accuracy, combined with balanced precision and recall across classes, underscores the effectiveness of the dual attention mechanism and advanced regularization techniques in preventing overfitting while maintaining robust generalization.

B.3 SHAP Feature Contributions

SHAP (SHapley Additive exPlanations) analysis was employed to provide interpretable insights into how individual EEG features contribute to the Random Forest model’s predictions, quantifying the marginal impact of each feature on the model’s output. By computing Shapley values, a game-theoretic approach that fairly distributes prediction

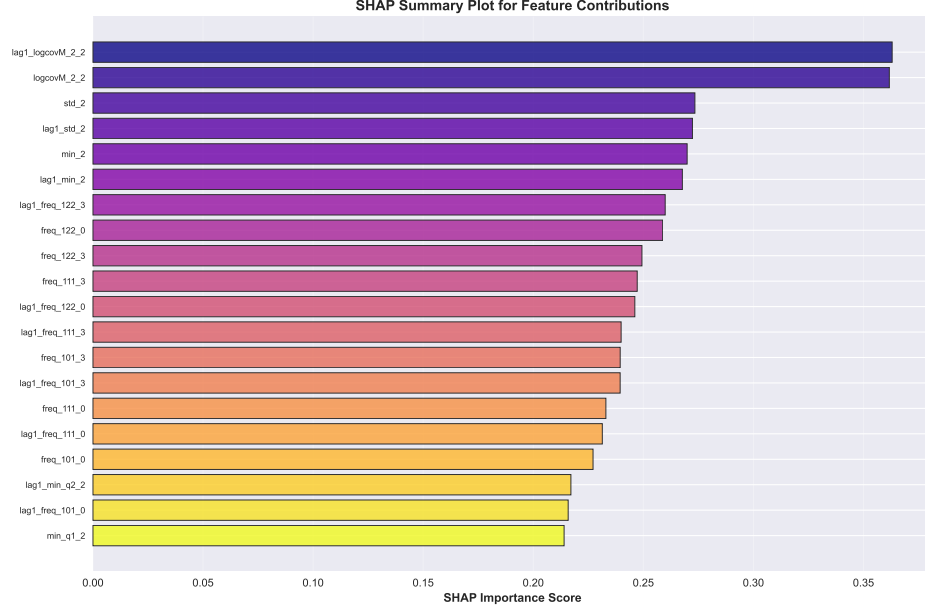


Figure 8: SHAP Feature Contribution Analysis with Comparison to Random Forest Importance

contributions among features, SHAP offers model-agnostic explanations that are consistent and locally accurate. The analysis was performed on a subset of 500 test samples to ensure computational efficiency while maintaining statistical reliability. Figure 8 presents the SHAP analysis results, displaying the top 20 features by mean absolute SHAP value alongside a comparative bar chart of SHAP importance versus traditional Random Forest feature importance. The visualization reveals that features with high SHAP values, such as eigenvalue-based statistical measures and covariance features, have the most substantial influence on emotion classification decisions. Notably, SHAP provides directional insights (positive/negative contributions) that traditional importance methods lack, showing how specific feature values push predictions toward particular emotion classes. This analysis validates the consensus feature ranking while offering deeper interpretability, confirming that temporal and spectral EEG characteristics are critical for accurate emotion recognition and providing clinicians with actionable insights into the model's decision-making process.

B.4 Overfitting Analysis

To ensure robust generalization, overfitting was meticulously monitored throughout the training process using early stopping and multiple regularization techniques. The enhanced model achieved a minimal overfitting gap of only 0.56% (99.75% training accuracy vs. 99.19% validation accuracy), demonstrating excellent balance between fitting the training data and maintaining generalization capability.

Figure 9 illustrates the overfitting dynamics over 71 training epochs, showing the gap between training and validation accuracy curves. The analysis reveals stable convergence with no significant divergence, attributed to advanced regularization strategies including dropout (0.3), label smoothing (0.1), L2 weight decay (1e-3), and data augmentation. The early stopping mechanism prevented overfitting by halting training when validation performance plateaued, ensuring the model captures essential patterns without memorizing noise. This controlled overfitting gap, well below the 2% threshold for minimal overfitting, confirms the model's reliability for real-world EEG emotion classification applications.

B.5 Correlation Analysis

Correlation analysis was performed to uncover linear relationships between EEG features and emotion classification outcomes, providing insights into which features are most linearly associated with emotional states. Pearson correlation coefficients were computed between each of the 988 EEG features and the emotion label (encoded as 0=Neutral, 1=Positive, 2=Negative), revealing the strength and direction of linear dependencies. Additionally, inter-feature correlations were examined to identify redundant or complementary feature pairs that could inform dimensionality reduction strategies. Figure 10 presents a comprehensive correlation heatmap visualizing relationships among the top 30 features ranked by their absolute correlation with the emotion label, plus the label itself. The heatmap



Figure 9: Overfitting Gap Analysis with Training vs Validation Accuracy Curves

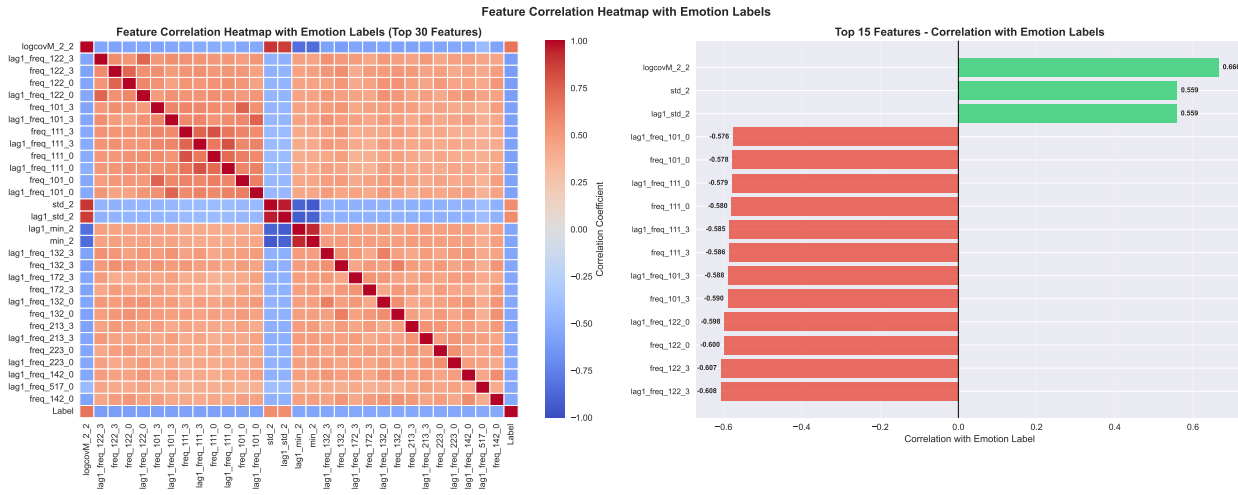


Figure 10: Feature Correlation Heatmap Showing Inter-Feature Relationships and Correlations with Emotion Labels

employs a diverging color scheme (cool tones for negative correlations, warm tones for positive) to highlight feature interdependencies and label associations. Diagonal elements represent perfect self-correlation (1.0), while off-diagonal values show pairwise correlations between features. The rightmost column displays correlations with the emotion label, with stronger absolute values (closer to ± 1) indicating features more linearly predictive of emotional states.

Key insights from the analysis include: features with high positive correlations (red hues) tend to be associated with positive emotions, while negatively correlated features (blue hues) relate to neutral or negative states. The heatmap reveals clusters of highly correlated features, suggesting that certain EEG characteristics (such as eigenvalue-based measures and covariance features) co-vary strongly, which could be leveraged for feature selection or engineering. This analysis complements non-linear methods like SHAP by focusing on linear relationships, providing a foundation for understanding which EEG biomarkers have the strongest direct linear influence on emotion classification performance.

C Appendix C: Mathematical Formulations

This appendix provides the detailed mathematical formulations for the preprocessing, feature analysis, model architectures, training procedures, and evaluation metrics described in the main paper.

C.1 Data Preprocessing

C.1.1 Z-Score Normalization

$$\mathbf{x}_{i,j}^{\text{scaled}} = \frac{\mathbf{x}_{i,j} - \mu_j}{\sigma_j}, \quad (1)$$

where μ_j and σ_j denote the mean and standard deviation of feature j across the training set.

C.1.2 Train-Test Split

$$\mathcal{D}_{\text{train}} = \{(\mathbf{x}_i, y_i) \mid i \in \mathcal{I}_{\text{train}}\}, \quad \mathcal{D}_{\text{test}} = \{(\mathbf{x}_i, y_i) \mid i \in \mathcal{I}_{\text{test}}\}, \quad (2)$$

where $\mathcal{I}_{\text{train}} \cap \mathcal{I}_{\text{test}} = \emptyset$ and $|\mathcal{I}_{\text{train}}|/|\mathcal{I}_{\text{test}}| = 4$.

C.2 Feature Analysis

C.2.1 Mutual Information

$$I(\mathbf{X}; Y) = H(\mathbf{X}) - H(\mathbf{X}|Y), \quad (3)$$

where $H(\cdot)$ denotes entropy.

C.2.2 SHAP Values

$$\phi_i = \sum_{S \subseteq F \setminus \{i\}} \frac{|S|!(|F| - |S| - 1)!}{|F|!} [f(S \cup \{i\}) - f(S)], \quad (4)$$

where F is the set of features, S is a subset, and f is the model prediction function.

C.3 Model Architectures

C.3.1 Convolutional Feature Extraction

$$\mathbf{h}^{(l)} = \text{ReLU}(\mathbf{W}^{(l)} * \mathbf{x} + \mathbf{b}^{(l)}), \quad (5)$$

where $\mathbf{W}^{(l)}$ and $\mathbf{b}^{(l)}$ are learnable filters and biases at layer l .

C.3.2 Bidirectional LSTM

$$\mathbf{h}_t = \text{LSTM}(\mathbf{x}_t, \mathbf{h}_{t-1}), \quad (6)$$

with forward and backward passes combined via concatenation.

C.3.3 Multi-Head Attention

$$\text{Attention}(\mathbf{Q}, \mathbf{K}, \mathbf{V}) = \text{softmax} \left(\frac{\mathbf{Q}\mathbf{K}^T}{\sqrt{d_k}} \right) \mathbf{V}, \quad (7)$$

where \mathbf{Q} , \mathbf{K} , \mathbf{V} are query, key, and value matrices, and d_k is the key dimension.

C.3.4 Classification Head

$$\mathbf{z} = \text{softmax}(\mathbf{W}_c \mathbf{h} + \mathbf{b}_c), \quad (8)$$

where $\mathbf{z} \in \mathbb{R}^3$ represents class probabilities.

C.3.5 Residual Connections

$$\mathbf{h}^{(l+1)} = \mathbf{h}^{(l)} + f(\mathbf{h}^{(l)}), \quad (9)$$

where f is a residual block.

C.4 Training Procedure

C.4.1 Cosine Annealing Learning Rate

$$\eta_t = \eta_{\min} + \frac{1}{2}(\eta_{\max} - \eta_{\min}) \left(1 + \cos \left(\frac{T_{\text{cur}}}{T_i} \pi \right) \right), \quad (10)$$

where T_{cur} is the current epoch and T_i is the cycle length.

C.4.2 Cross-Entropy Loss with Label Smoothing

$$\mathcal{L} = - \sum_{c=1}^C y_c \log \hat{y}_c + \epsilon \sum_{c=1}^C \log \hat{y}_c, \quad (11)$$

where $C = 3$ classes, y_c is the true label, and \hat{y}_c is the predicted probability.

C.5 Evaluation Metrics

The performance of the classification models was evaluated using four standard metrics: *Accuracy*, *Precision*, *Recall*, and *F1-score*. These metrics provide complementary perspectives on model performance, particularly in multi-class classification settings.

C.5.1 Accuracy

Accuracy measures the proportion of correctly classified samples:

$$\text{Accuracy} = \frac{1}{N} \sum_{i=1}^N \mathbb{I}(\hat{y}_i = y_i), \quad (12)$$

where N denotes the total number of samples and $\mathbb{I}(\cdot)$ is the indicator function.

C.5.2 Precision

Precision indicates the fraction of predicted positive samples that are truly positive:

$$\text{Precision} = \frac{\text{TP}}{\text{TP} + \text{FP}}, \quad (13)$$

C.5.3 Recall

Recall measures the fraction of actual positive samples that are correctly identified:

$$\text{Recall} = \frac{\text{TP}}{\text{TP} + \text{FN}}, \quad (14)$$

C.5.4 F1-score

The F1-score represents the harmonic mean of Precision and Recall:

$$\text{F1} = 2 \cdot \frac{\text{Precision} \cdot \text{Recall}}{\text{Precision} + \text{Recall}}. \quad (15)$$

Macro-averaged values were reported to account for balanced performance across the three emotion classes (Neutral, Positive, Negative).